

## LA-UR-15-24146

Approved for public release; distribution is unlimited.

Title: ENHANCEMENTS TO THE BUILT-IN MCNP6 DETECTOR RESPONSE FUNCTIONS

Author(s): McMath, Garrett Earl  
Mckinney, Gregg Walter

Intended for: INMM 56th Annual Meeting, 2015-07-12/2015-07-16 (Indian Wells,  
California, United States)

Issued: 2015-06-04

---

**Disclaimer:**

Los Alamos National Laboratory, an affirmative action/equal opportunity employer, is operated by the Los Alamos National Security, LLC for the National Nuclear Security Administration of the U.S. Department of Energy under contract DE-AC52-06NA25396. By approving this article, the publisher recognizes that the U.S. Government retains nonexclusive, royalty-free license to publish or reproduce the published form of this contribution, or to allow others to do so, for U.S. Government purposes. Los Alamos National Laboratory requests that the publisher identify this article as work performed under the auspices of the U.S. Department of Energy. Los Alamos National Laboratory strongly supports academic freedom and a researcher's right to publish; as an institution, however, the Laboratory does not endorse the viewpoint of a publication or guarantee its technical correctness.

# ENHANCEMENTS TO THE BUILT-IN MCNP6 DETECTOR RESPONSE FUNCTIONS

G. E. McMath and G. W. McKinney

*Los Alamos National Laboratory, P.O. Box 1663 MS P939, Los Alamos, NM, 87545  
gem@lanl.gov, gwm@lanl.gov*

## ABSTRACT

*Recent interest in modeling and simulation of detector systems has led to several enhancements to the radiation transport code, MCNP6. The most recent improvement to the detector modeling capability has been the expansion of the built-in detector response functions. MCNP first implemented dose functions in MCNPX 2.4.0 and since then specific detector types have been added. The next release of MCNP6 will include response functions for 5 new neutron detector types along with the previously built-in photon detector responses. This paper will demonstrate the use of the new response functions as well as provide benchmarking.*

## INTRODUCTION

As the use of modeling codes to design experiments and detector systems increases, so does the importance of accurately producing detector responses. Detector response functions (DRFs) can be used in a variety of ways such as: providing variance reduction by reducing transport, modeling physics not available in the code, allowing for direct comparison to experimental data, and simulating data analysis methods such as pulse shape discrimination (PSD). The DRFs recently added to MCNP6 [1] provide several of these features. Most importantly they allow the calibration of modeled detectors to actual detectors. Once this calibration is done, any number of virtual experiments can be carried out with the results matching experimental data.

This approach of varying parameters in a virtual space to inform real world decisions has been gaining popularity as the accuracy and capabilities of transport codes continue to improve. In particular, the Department of Homeland Security's (DHS) Domestic Nuclear Detection Office (DNDO) has supported many of these features in order to inform the design and characterization of detector systems prior to deployment. In the effort to support this mission, DRFs have been added to MCNP6 and will be available in the next release of the code. This paper will cover the fundamental use of the MCNP6 detector response functions as well as provide benchmarking that have been performed.

## MCNP6 IMPLEMENTATION

The first implementation of the detector response function was in MCNPX 2.4.0 and only included photons detectors until this latest upgrade. The fundamental theory behind the DRFs is based on which detector type is chosen. The next release of MCNP6 will include three types of detectors: gas proportional counters, scintillators, and semi-conductors.

For scintillation detectors, Birks' Law [2] is used to produce light yield output. The formula assumes proportionality between light yield and energy loss multiplied by scintillation efficiency,  $S$ . Birks also added a term to account for quenching containing adjustable parameters,  $k_B$ , to fit experimental data, see Eq 1.

$$\frac{dL}{dx} = \left(\frac{dL}{dE}\right) \left(\frac{dE}{dx}\right) = \left(\frac{S}{1 + k_B \frac{dE}{dx}}\right) \frac{dE}{dx} \quad (1)$$

The light yield per energy deposition term of Eq. 1 is the DRF while the second term is already computed by MCNP6 as the stopping power. The free parameters in Eq. 1 are reduced to two constants for implementation into MCNP6, see Eq. 2.

$$\frac{dL}{dE} = \frac{C_0}{1 + C_1 \frac{dE}{dx}} \quad (2)$$

$C_0$  in Eq. 2 is determined by requiring the light yield be unity for a 1 MeV electron and  $C_1$  can be found in literature or fit from experimental data.

For gas detectors the response is the charge per source particle ( $Q$ ) in picocoulombs ( $pC$ ). This allows charge binning to incorporate pre-amplifier thresholds. This is calculated by the charged particle energy deposition in MeV ( $E$ ) multiplied by the inverse of the gas work function in MeV per ion pair ( $C_0$ ), the electron charge per ion pair, and the E-field multiplication factor which can be modified to match a specific detector ( $C_1$ ), see Eq. 3. Semi-conductors are treated in the same way the only difference typically being a smaller work function.

$$Q = E \left( \frac{1.602177e-7 \frac{pC}{ion\ pair}}{C_0} \right) C_1 \quad (3)$$

Two parameters,  $C_0$  and  $C_1$ , are used for all the DRFs.  $C_0$ , at this time, cannot be directly changed outside of the source code file, (`fluence_to_dose.F90`). For scintillation detectors  $C_0$  is a normalization constant to ensure output in MeVee, (electron equivalent MeV). For gas and semi-conductor detectors  $C_0$  is the work function in MeV/ion pair. This work function cannot be directly changed, however, Eq. 3 shows that it may be incorporated into  $C_1$ , which can be modified by an input deck. Eq. 4 shows the simple relation required to change both the default  $C_0$  (work function) and  $C_1$  (multiplication factor,  $M$ ) for gas and semi-conductor detectors only.

$$C_{1\ total} = C_{0\ default} \left( \frac{C_{1\ new}}{C_{0\ new}} \right) \quad (4)$$

$C_1$  can be modified by appending an underscore to the detector name followed by the desired quantity. For example, the default values for  $C_0$  and  $C_1$  for the HE3-1 detector are  $4.1e-7$  MeV/ion

pair and 100 respectively. By entering, he3-1\_20, the multiplication factor  $C_1$  is changed to 20. This can be used to alter the default  $C_0$  for gas and semi-conductors detectors as can be seen in Eq 4. The definitions and defaults of the two parameters for all detectors can be found in Table I.

TABLE I. Built-in detector parameter in MCNP6

Detector Type	Detector Name	Primary Particle Type(s)	Response Parameter*	$C_1$ Default Value	$C_0$ Default Value for 1 <sup>st</sup> Primary Particle
<sup>3</sup> He	HE3-1	Proton, Triton, Helion	M	100	41.0 eV/ion pair [3]
BF <sub>3</sub>	BF3-1	Alpha, Lithium	M	100	36.0 eV/ion pair [4]
Li Glass	LIG-1	Triton, Alpha	QF	5.0e-4 cm/MeV	1.000296
LiI	LII-1	Triton, Alpha	QF	5.0e-4 cm/MeV	1.000149
ZnS+LiF	ZNS-1	Triton, Alpha	QF	5.0e-4 cm/MeV	1.000190
NaI	NAI-1	Electron	QF	3.4e-4 cm/MeV	1.000114 [5]
BGO	BGO-1	Electron	QF	6.5e-4 cm/MeV	1.000111 [6]
CsI	CSI-1	Electron	QF	1.5e-4 cm/MeV	1.000040 [6]
BC-400	BC4-1	Electron	QF	4.6e-3 cm/MeV	1.008349 [7]
HPGe	HPG-1	Electron	G	1.0	3.0 eV/ion pair [8]

\* M=multiplication, QF=quenching factor, G=gain

The built-in DRFs are designed for use with F6 energy deposition tallies in conjunction with either a DF card or with FT8 PHL tally. The DF card IC option specifies which standard dose function to use with a corresponding tally. In order to use the DRFs, set the DF card's IC value corresponding to the relevant F6 tally equal to one of the detector names in Table I. A more standard approach is to use the FT8 PHL tally to sum relevant F6 tallies together and then apply the DRF. For example a <sup>3</sup>He detector has three relevant charged particles that contribute to the signal. Three F6 tallies can be made for each of the relevant particles and summed together in a PHL tally with the HE3-1 DRF. Since the DRF changes energy [MeV] to charge [pC] for gas detectors an E card can be used to bin the charge from the detector and designate a charge threshold for a particular detector. This approach was taken for a suite of Centronic <sup>3</sup>He detector tubes in order to benchmark the capability.

### HE3-1 BENCHMARKING

Centronic lists the sensitivities for all of its <sup>3</sup>He detectors in counts per second per unit of thermal neutron flux (cps/nv) [9]. A subset of the detectors with diameters ranging from 13 mm to 38 mm, active lengths ranging from 97 mm to 1250 mm, and fill pressures from 2 atm to 10 atm were modeled and run in a unit thermal neutron flux to compare sensitivities. Communications with Centronic engineers provided many of the required parameters such as anode radius, material compositions, gas multiplication factor, and volume fraction of quench gas. The simulations were run with a gas multiplication factor ( $C_1$ ) of 20 and a charge threshold of 0.016 pC. Centronic did not give a definitive charge threshold, however, they said it was approximately 0.015 pC. The best optimized threshold for all simulations was 0.016 pC which seemed reasonable. The results of the simulations can be seen in Table II.

Table II. Results of Centronic detector simulations using HE3-1 20 DRF\*

<b>13 mm Diameter</b>	<b>Active Length [mm]</b>	<b>2 atm</b>	<b>4 atm</b>	<b>6 atm</b>	<b>8 atm</b>	<b>10 atm</b>
	76	2.02	3.80	5.10	6.10	6.90
MCNP6 DRF [cps/nv]		2.01	3.90	5.18	6.08	6.72
Relative Error [%]		0.63	2.66	1.58	0.38	2.55
	150	4.30	7.60	10.00	12.00	14.00
MCNP6 DRF [cps/nv]		4.04	7.77	10.28	12.06	13.39
Relative Error [%]		6.06	2.18	2.77	0.52	4.37
	249	7.10	13.00	17.00	20.00	23.00
MCNP6 DRF [cps/nv]		6.79	12.88	17.01	20.00	22.20
Relative Error [%]		4.34	0.92	0.06	0.01	3.47
	508	14.00	25.00	34.00	40.00	46.00
MCNP6 DRF [cps/nv]		13.96	26.34	34.65	40.74	45.20
Relative Error [%]		0.27	5.36	1.91	1.85	1.73
<b>25 mm Diameter</b>	<b>Active Length [mm]</b>	<b>2 atm</b>	<b>4 atm</b>	<b>6 atm</b>	<b>8 atm</b>	<b>10 atm</b>
	97	9.7	16	19	21	22
MCNP6 DRF [cps/nv]		10.59	16.29	19.28	20.87	21.79
Relative Error [%]		9.20	1.80	1.45	0.64	0.97
	127	13	21	25	28	30
MCNP6 DRF [cps/nv]		13.84	21.27	25.17	27.25	28.48
Relative Error [%]		6.47	1.31	0.67	2.66	5.07
	150	15	24	30	33	35
MCNP6 DRF [cps/nv]		16.19	24.92	29.52	32.02	33.52
Relative Error [%]		7.91	3.84	1.61	2.96	4.24
	249	25	40	50	55	58
MCNP6 DRF [cps/nv]		26.77	41.23	48.82	53.04	55.55
Relative Error [%]		7.07	3.07	2.36	3.56	4.23
	500	50	81	99	110	117
MCNP6 DRF [cps/nv]		53.53	82.34	97.51	106.09	111.21
Relative Error [%]		7.06	1.65	1.51	3.56	4.95
	1001	101	161	198	220	234
MCNP6 DRF [cps/nv]		107.06	164.42	194.89	212.15	222.35
Relative Error [%]		6.00	2.12	1.57	3.57	4.98
	1250	126	202	248	275	292
MCNP6 DRF [cps/nv]		133.56	205.12	243.28	264.93	277.68
Relative Error [%]		6.00	1.54	1.90	3.66	4.91
<b>38 mm Diameter</b>	<b>Active Length [mm]</b>	<b>2 atm</b>	<b>4 atm</b>	<b>6 atm</b>	<b>8 atm</b>	<b>10 atm</b>
	150	30	45	51	54	56
MCNP6 DRF [cps/nv]		32.95	45.20	50.12	52.26	53.30
Relative Error [%]		9.83	0.45	1.72	3.22	4.82
	249	51	74	85	91	93
MCNP6 DRF [cps/nv]		54.08	74.53	82.89	86.55	88.37
Relative Error [%]		6.03	0.72	2.48	4.89	4.98
	500	101	149	171	181	186
MCNP6 DRF [cps/nv]		107.41	148.32	165.33	173.02	176.78
Relative Error [%]		6.35	0.45	3.31	4.41	4.95
	1001	202	297	342	363	372
MCNP6 DRF [cps/nv]		213.85	295.81	330.08	345.59	353.32
Relative Error [%]		5.87	0.40	3.48	4.80	5.02

\* All MCNP6 simulation tally run with 1e8 histories resulting in less than 1% relative error

Three higher fidelity simulations were performed for the different diameter tubes to compare wall effects. The spectra of the simulations can be seen in Figure 1. The two discrete wall effects can be clearly seen corresponding to the 191 keV (0.015 pC) triton edge and 573 keV (0.045 pC) proton edge. The full energy peak which corresponds to 764 keV (0.06 pC) for thermal neutrons is also easily distinguished. As expected the peak to total ratio increases for larger diameter tubes, see Table III.

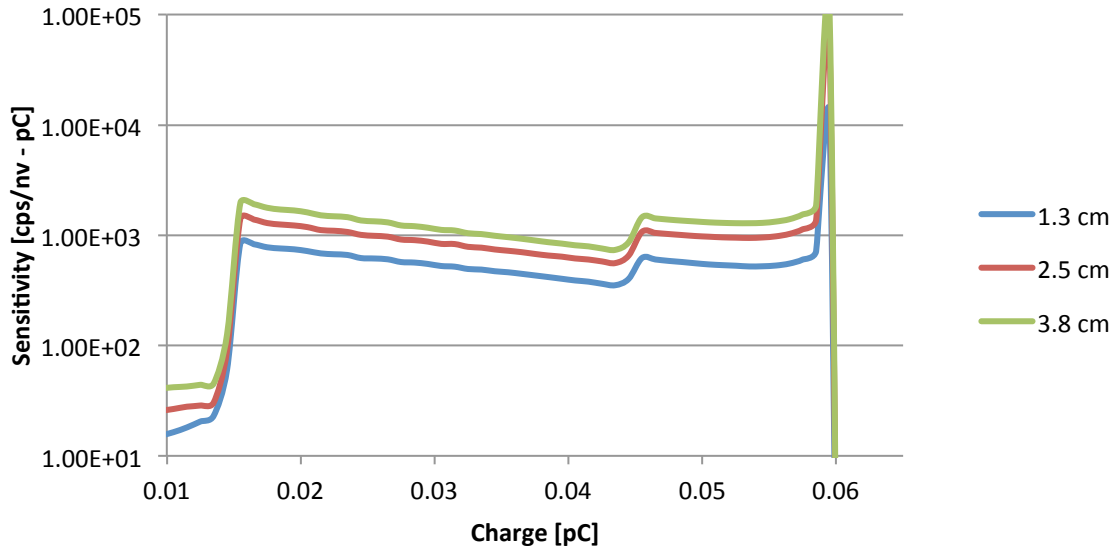


Figure 1. Charge spectrum of three diameters of 50 cm long  $^3\text{He}$  tubes illustrating the wall effects from proton and triton recoil as well as the full energy peak. As expected the full energy peak to wall effect ratio diminishes as the diameter increases.

Table III. Peak to total ratios for 50 cm active length  $^3\text{He}$  tubes

Diameter [cm]	Peak [cps/nv]	Total [cps/nv]	Ratio
1.3	1.09E+01	3.47E+01	3.13E-01
2.5	5.75E+01	9.75E+01	5.90E-01
3.8	1.11E+02	1.65E+02	6.73E-01

## CONCLUSION

New detector response functions have been added to the radiation transport code MCNP6. These new DRFs will be available with the next release of the code. Benchmarking is ongoing but the initial results have compared very well with a manufacturer’s reported specifications. For 75 different models of  $^3\text{He}$  tubes the average relative error was 3.3% between the modeled and reported sensitivities. The errors were consistently lower for the mid pressure models, indicating there may have been a slightly different multiplication factor or charge threshold used for the characterization of the 2 and 10 atm cases. These new features allow for a direct comparison to reported or experimental results without the use of post-processing codes.

## ENDNOTES

This work has been supported by the U.S. Department of Homeland Security, Domestic Nuclear Detection Office, under competitively awarded contract/IAA HSHQDC-12-X-00251. This support does not constitute an express or implied endorsement on the part of the Government.

## REFERENCES

1. D. B. Pelowitz, A.J. Fallgren, and G. E. McMath editors, "MCNP6 User's Manual, Version 6.1.1beta," LANL report LA-CP-14-00745 (2014).
2. J. B. Birks, *The Theory and Practice of Scintillation Counting*, Pergamon Press, Oxford, 1964
3. D. Mazed, S. Mameri, and R. Ciolini, "Design parameters and technology optimization of  $^3\text{He}$ -filled proportional counters for thermal neutron detection and spectrometry applications," *Radiation Measurements*. 47, 577-587 (2012).
4. T. E. Bortner and G. S. Hurst, "Ionization of Pure Gases and Mixtures of Gases by 5-MeV Alpha Particles," *Phys. Rev.* 93, 1236-1241 (1954).
5. V. I. Tretyak, "Semi-empirical calculation of quenching factors for ions in scintillators," *Astroparticle Physics*. 33, 40-53 (2010).
6. V. Avdeichikov, B. Jakobsson, A. A. Nikitin, P. V. Nomokonov, A. Wegner, "Systematics in the light response of BGO, CsI(Tl) and GSO(Ce) scintillators to charged particles," *Nuclear Instruments and Methods in Physics Research Section A*. 484, 251-258 (2002).
7. A. Menchaca,-Rocha, M. Buenerd, L. Gallin-Martel, F. Ohlsson-Malek, T. Thuillier, "Response measurements of NE102 to  $Z = 2-6$  ions at  $E/A = 0.15-1.5$  GeV, and predictions for higher  $Z$ 's," *Nuclear Instruments and Methods in Physics Research Section A*. 438, 322-332 (1999).
8. S. H. Byun, "Radiation & Radioisotope Methodology," Chp. 7 Semiconductor Detectors (2014)
9. " $^3\text{He}$  Neutron Proportional Counters." *Centronic Helium-3 Neutron Proportional Counters*. Centronic LTD, 2011. Web. 01 June 2015. <http://www.centronic.co.uk/helium.htm>